Modulated phases in $NaNbO_3$: Raman scattering, synchrotron x-ray diffraction, and dielectric investigations

2005 J. Phys.: Condens. Matter 17 4977

(http://iopscience.iop.org/0953-8984/17/33/003)

INSTITUTE OF PHYSICS PUBLISHING JOURNAL OF PHYSICS: CONDENSED MATTER

J. Phys.: Condens. Matter **17** (2005) 4977–4990 doi:10.1088/0953-8984/17/33/003

Modulated phases in $NaNbO_3$: Raman scattering, synchrotron x-ray diffraction, and dielectric investigations

Yu I Yuzyuk[1,2,3], P Simon[1], E Gagarina[1,2,3], L Hennet[1], D Thiaudière[1,4], V I Torgashev[2,3], S I Raevskaya[2,3], I P Raevskii[2,3], L A Reznitchenko[2,3] and J L Sauvajol[5]

[1] Centre de Recherches sur les Materiaux à Haute Temperature, CNRS UPR 4212, F45071, Orléans, France
[2] Institute of Physics, Rostov State University, Stachki 194, Rostov-on-Don, 344090, Russia
[3] Faculty of Physics, Rostov State University, Zorge 5, Rostov-on-Don, 344090, Russia
[4] LURE, CNRS, Centre Universitaire Paris-Sud, BAT 209D, F91198, Orsay, France
[5] Laboratoire des Colloïdes, Verres et Nanomatériaux, UMR CNRS 5587, Université Montpellier II, 34095 Montpellier Cedex 5, France

Received 11 May 2005, in final form 19 July 2005
Published 5 August 2005
Online at stacks.iop.org/JPhysCM/17/4977

Abstract

Raman spectra of sodium niobate ($NaNbO_3$) were obtained in all phases and revealed a significant disorder in the high-temperature U, T2 and T1 phases and a complicated folding of the Brillouin zone at the transitions into modulated S, R, P and N phases associated with the competitive zone-boundary soft modes (in-phase and out-of phase octahedral tilts) along the M–T–R line. An extensive Raman study combined with x-ray diffraction (XRD) and dielectric measurements confirmed the presence of the incommensurate (INC) phase in sodium niobate. XRD experiments revealed the invar effect in the temperature interval 410–460 K corresponding to the INC phase associated with rotations of the NbO_6 octahedra modulated along the *b*-direction. Our experiments suggest that the phase P consists of three phases: monoclinic (P_m) between 250 and 410 K, INC between 410 and 460 K, and orthorhombic (P_o) between 460 and 633 K. At the low-temperature transition to the ferroelectric rhombohedral N phase all folded modes originating from the M- and T-points of the Brillouin zone abruptly disappear, Raman spectra in the N phase become much simpler and all peaks were assigned.

1. Introduction

Sodium niobate ($NaNbO_3$, hereafter NN) exhibits an unusually large number of successive phase transitions and is the most complex perovskite ferroelectric known [1–3]. This material exhibits both ferroelectric and antiferroelectric properties [4], and is therefore

of particular interest in the study of ferroelectrics. The high-temperature phase above 913 K is a simple prototype cubic perovskite. The crystal structures of the low-symmetry phases were systematically studied by means of x-ray diffraction (XRD) [5–10]. The seven phases of NN were listed by Megaw [11] in 1974: U (paraelectric O_h^1, $Z = 1$) $\rightarrow$ 913 K $\rightarrow$ T2 (paraelectric, D_{4h}^5, $Z = 2$) $\rightarrow$ 848 K $\rightarrow$ T1 (paraelectric, D_{2h}^{17}, $Z = 4$) $\rightarrow$ 793 K $\rightarrow$ S (paraelectric, D_{2h}^{13}, $Z = 8$) $\rightarrow$ 753 K $\rightarrow$ R (antiferroelectric, D_{2h}^{13}, $Z = 24$) $\rightarrow$ 633 K $\rightarrow$ P (antiferroelectric, D_{2h}^{11}, $Z = 8$) $\rightarrow$ 173 K $\rightarrow$ N (ferroelectric, C_{3v}^6, $Z = 2$). However, a whole phase transition sequence even at atmospheric pressure is still not absolutely certain. Dénoyer *et al* [12] proposed that the multiplicity of the unit cell in the S phase reported earlier [8] is not correct. Recently, Darlington and Knight [13] have shown that the symmetry of the room-temperature phase P is monoclinic rather than orthorhombic. Moreover, they found that the multiplicities of the pseudocubic cells describing the orthorhombic S and R phases are larger with respect to those reported in the previous literature (see table 1 in [13]). An additional phase transition at about 463 K was proposed from Raman [14] and dielectric studies [15]. Very recently, an incommensurate (INC) phase in the temperature range 410–460 K was established from the XRD, dielectric, and dilatometric studies of NN single crystals and ceramics [16].

NN-based solid solutions exhibit ferroelectric, antiferroelectric [17–19] and relaxor properties [20], which are of interest for practical applications. The phase diagrams of (K, Na)NbO_3 and (Li, Na)NbO_3 are very complicated and contain a large number of phases [17–19]. The primary mechanisms and numerous phase transitions in NN-based solid solutions are not yet understood because the complete phase transition sequence and order parameters determining all structural changes in NN are still unknown. In the present work we performed an extensive Raman study combined with XRD and dielectric measurements with the aim to clarify the phase transition sequence in NN. Raman spectra were obtained in all phases and revealed a complicated folding of the Brillouin zone (BZ) at phase transitions. Our experiments suggest that the well-known phase P consists of three phases: monoclinic (P_m) between 250 and 410 K, INC between 410 and 460 K, and orthorhombic (P_o) between 460 and 633 K. All peaks in the Raman spectra of the low-temperature ferroelectric phase N were assigned.

2. Literature review

The two highest-temperature phase transitions to the nonpolar phases correspond to the tiltings of the oxygen octahedra and are associated with soft phonons at the BZ boundary [1]. The U–T2 transition is caused by the condensing of the M_3 soft mode at the M-point ($\mathbf{q} = \frac{1}{2}\mathbf{b}_1 + \frac{1}{2}\mathbf{b}_2$) of the cubic BZ. This mode involves in-phase octahedral rotation about [001] and induces tetragonal phase. Using Glazer's notations [21] the corresponding tilting scheme is $a^0b^0c^+$. The next phase transition T2–T1 at 848 K is associated with the soft mode at the R-point ($\mathbf{q} = \frac{1}{2}\mathbf{b}_1 + \frac{1}{2}\mathbf{b}_2 + \frac{1}{2}\mathbf{b}_3$) of cubic BZ. Since the R_{25} mode corresponds to octahedral rotation in the opposite sense, the tilting scheme in the orthorhombic T1 phase is $a^-b^0c^+$, where the superscripts denote in-phase (+), anti-phase (−) or zero (0) tilts, respectively. The diffuse x-ray scattering studied at the R- and M-points was found to be strongly anisotropic and distributed along ⟨100⟩ reciprocal rods connecting the R- and M-points [22]. This anisotropy was reasonably explained assuming that the low-frequency zone-boundary phonons from the line T ($\mathbf{q} = \frac{1}{2}\mathbf{b}_1 + \frac{1}{2}\mathbf{b}_2 + \mu\mathbf{b}_3$) lying between the R- and M-points are also involved and give rise to strong diffuse scattering. Later, x-ray diffuse and inelastic neutron scattering studies also revealed diffuse scattering concentrated along the lines joining the R- and M-points in the cubic phase [12, 23]. Darlington [24–26] has performed a normal mode analysis and

determined the primary order parameters of the transitions to the T2 and T1 phases. The phase transitions between the S, R and P phases are less well investigated, and substantial unit cell enlargements and complicated octahedral tilting in the alternating layers are not yet understood. It is worth noting that the low-temperature transition to the rhombohedral N phase is caused by the condensation of all three components of the R_{25} soft mode from the R-point accompanied by the softening of the zone-centre (Γ-point) polar F_{1u} mode, which corresponds to Nb displacements.

The temperature dependence of the zone-centre polar lattice vibrations, including a soft mode, in the cubic phase of NN single crystal was studied by infrared (IR) reflectivity spectroscopy [27]. The lowest-frequency transverse optic (TO) mode displayed a soft-mode behaviour in the cubic paraelectric phase between 106 and 91 cm^{-1} on cooling down from 1250 to 915 K. In addition, on cooling towards the U–T2 transition, Gervais *et al* [27] have observed the progressive passage from the underdamped soft-mode regime with a resolved central peak to the highly overdamped soft-mode regime with unresolved central peak. These features imply that a simple picture of the U–T2 phase transition associated with the condensation of a soft mode at the M-point of the BZ is incomplete.

Husson and Repelin [28] have analysed IR and Raman spectra of single-crystalline NN at room temperature, and a detailed mode assignment was proposed. Wang *et al* [14] have studied Raman spectra of polycrystalline NN from room temperature up to 753 K. These authors have observed the P–R phase transition at 649 K, in good agreement with the results reported in literature. In addition, they found a series of evident changes in the Raman spectra at about 363 K, and a new intermediate phase, stable in the temperature range 363–633 K, has been proposed. The antiferroelectric to ferroelectric phase transition between P and N phases in polycrystalline NN was investigated by Raman scattering between 295 and 10 K [29]. The P–N transition occurred at 185 K on cooling and at 210 K on heating. Coexistence of P and N phases was revealed down to 43 K. Although two modes at 155 and 121 cm^{-1} exhibited softening on cooling the P–N transition was not considered to be the displacive type. Lima *et al* [30] reported Raman spectra of NN ceramics prepared by a new chemical route. Their Raman spectra obtained in the temperature range 15–297 K revealed two diffuse phase transitions at 250 and at 95 K. Recently [31], polarized Raman spectra of NN single crystals, in both P and R phases, were investigated from room temperature up to 713 K. These authors revealed the presence of a strong quasi-elastic scattering below a low-frequency zone-centre phonon. The P–R phase transition was interpreted in terms of a mechanism induced by relaxing dipoles around off-centre Nb ions, reflecting an order–disorder character of this transition. Very recently, Jiménez *et al* [32] have reported dielectric and Raman spectroscopic studies on Li–Na niobate ceramics. According to these authors, the temperature evolution of the Raman spectra in the low-frequency (50–180 cm^{-1}) region evidenced small structural changes in the 450–560 K temperature interval that indicate the coexistence of two close structural phases with similar energies that should correspond to a ferroelectric Q phase and an antiferroelectric P phase.

3. Experimental details

Platelike ($0.3 \times 2 \times 2$ mm^3) colourless transparent NN single crystals were grown from flux with the use of the Na_2CO_3–B_2O_3 system as a solvent. High-density (99.8%) NN ceramics were prepared by the solid-state reaction of stoichiometric quantities of Na_2CO_3 (99.8%) and Nb_2O_5 (98.7%). All ceramic samples were synthesized using a two-stage annealing at 850–900 °C for 4–5 h at each stage. The components were mixed in ethanol to avoid hydrolysis and milled in water. Sintering was carried out at 1050–1250 °C and pressure 20–40 MPa for

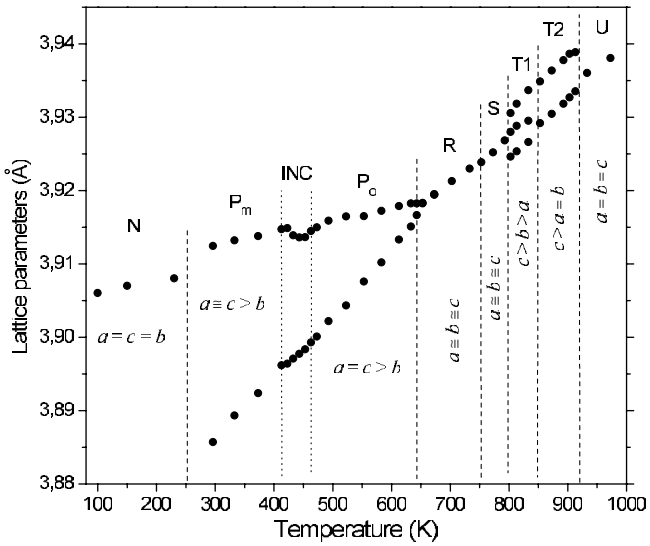

Figure 1. Temperature dependences of the perovskite subcell parameters in NN. Dashed lines mark phase transition temperatures (on heating). Dotted lines mark the invar effect.

40 min. Fine-granular powders for XRD measurements were prepared by crushing ceramic specimens.

Synchrotron XRD patterns were obtained on the H10 beamline [33] at LURE/DCI (Orsay, France). A monochromatic radiation ($\lambda = 1.304\,23$ Å) was obtained by using a double-crystal Si(111) monochromator. Powder diffraction measurements were recorded in the Bragg–Brentano geometry using a gas-filled INEL CPS120 detector. The beam size at the sample position was 4 mm horizontally and 10 μm vertically. High-temperature investigations were performed using a furnace with temperature stability ± 0.5 K. The powders were placed in boron nitride crucibles. A continuous furnace oscillation was used to eliminate the preferred orientation effects and to improve the particle size statistics. The unit cell parameters were determined using structure-free fits (FULLPROF software [34]).

Raman spectra were excited with the polarized light of an Ar^+ laser ($\lambda = 514.5$ nm) and analysed using a Jobin Yvon T64000 spectrometer equipped with a charge-coupled device. All spectra were obtained in backscattering geometry using a microprobe device that allows the incident light to be focused on the sample as a spot of about 3 μm in diameter. The low-temperature measurements were performed using a helium micro cryostat (Oxford) with a temperature stability of about ± 0.5 K. For high-temperature measurements we used a Linkam TS 1500 hot stage with a temperature stability of ± 1.5 K. The dielectric permittivity was measured at frequencies 1–100 kHz using an alternate-current P5083 LCR-meter.

4. Results and discussion

Powder XRD diffraction experiments were performed in the temperature interval 77–980 K. Figure 1 shows the temperature dependences of the perovskite subcell parameters a, b, and c. The phase transition temperatures correlate well with those reported in the literature [10, 11], and all known seven phases can be distinguished. According to neutron powder diffraction data reported by Darlington and Knight [13], the multiplicities of the unit cells describing the orthorhombic S and R phases are both $2a \times 6b \times 4c$ ($a \sim b \sim c$), and not $2a \times 2b \times 2c$ and $2a \times 6b \times 2c$ as was reported previously [5, 8, 10]. It is worth noting that the unit cell parameters are very close and the multiplicities $2a \times 6b \times 4c$ and $2a \times 4b \times 6c$ cannot be

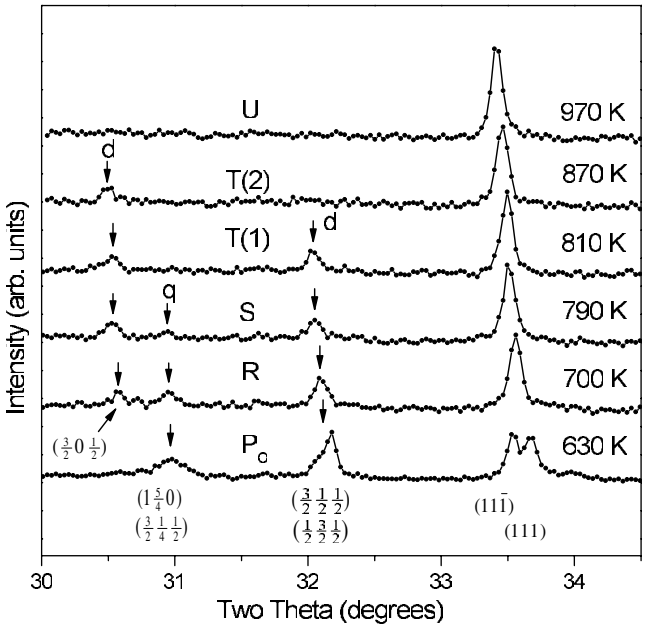

Figure 2. Portion of the synchrotron diffraction patterns at selected temperatures. The indices of the superlattice reflections referred to the pseudocubic perovskite subcell are given in brackets. Symbols q and d mark superlattice reflections due to the perovskite subcell quadrupling and doubling, respectively.

distinguished. As shown in figure 2, the superlattice reflections due to the quadrupling of the perovskite subcell were observed in the R and S phases. The intensities of the reflections due to the six-fold increase of the perovskite subcell were too weak to be detected in our XRD powder diffraction experiments. Another important feature (never reported before) is that in the P phase, both a and c parameters are nearly temperature independent in the 410–460 K interval. The observed invar effect is a signature of the INC modulation. In the temperature dependence of the unit cell parameters a change of the slope just below 410 K is evident. Moreover, in the room-temperature XRD patterns, the $h00$ reflections are slightly broader compared to the $0h0$ ones. This feature could be interpreted as an evidence of the weak monoclinic distortion $a \neq c$. On heating from room temperature up to 460 K the difference in the width of these reflections vanishes gradually, implying that the unit cell is orthorhombic ($a = c > b$) above 460 K. Therefore, one can assume that the well-known phase P consists of three phases, monoclinic (P_m), INC, and orthorhombic (P_o), as shown in figure 1. No change of the unit cell multiplicity between P_o and P_m phases was detected. Additional high-resolution single-crystalline experiments are required to confirm the above suggestion.

Most NN crystals are twinned and exhibit very complicated domain structure at room temperature [35]. Due to very strong depolarization of the incident and scattered light inside the polydomain single crystal, the Raman spectra are totally depolarized and usually no discrimination between parallel and crossed polarized spectra can be observed at room temperature. Using a micro-Raman technique one can obtain partially polarized spectra in a particular sample area where the twins are large enough. However, all lines are observed simultaneously and only their relative intensity depends on the polarization of the incident/scattered light. Due to this circumstance, detailed symmetry assignments of the

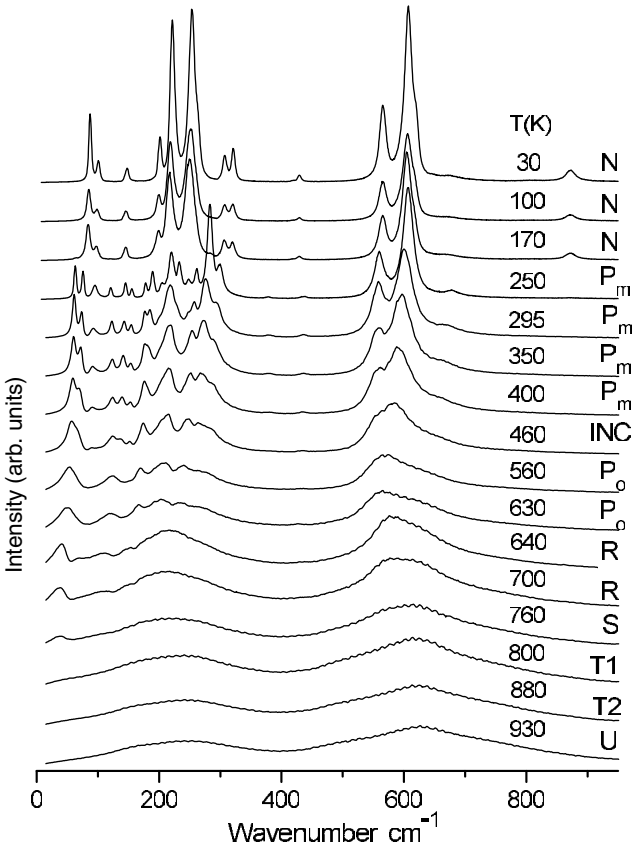

Figure 3. Raman spectra of an NN single crystal at selected temperatures. All spectra are corrected for the temperature factor.

phonon modes are not possible. Raman spectra of NN single crystals and ceramics were studied in the temperature range 30–980 K. All known phase transitions were observed in both kinds of samples. In the case of ceramics all phase transitions are slightly diffused, probably due to phase coexistence, and slightly shifted in temperature scale. Due to Rayleigh scattering the soft-mode behaviour is less pronounced in ceramic samples, and in the following we discuss parallel-polarized (VV) Raman spectra obtained in single crystals.

The Raman spectra of an NN single crystal at selected temperatures are presented in figure 3. It is worth noting that the Raman spectra in U, T2 and T1 phases are quite similar and consist of two broad asymmetrical bands centred at about 230 and 620 cm^{-1}. These bands do not show any remarkable temperature variation and very likely arise due to disorder in the high-temperature phases. No changes in Raman spectra were found at transitions to T2 and T1 phases. Similar disorder-induced broad features (mainly the one-phonon density of states) were previously observed in $KNbO_3$ and $BaTiO_3$ crystals [36, 37], and attributed to the off-centering of the B cation in the framework of the eight-site model [38]. Therefore, the presence of these bands suggests significant disorder in the high-temperature phases of NN.

Due to unit cell doubling along two directions at the phase transition U($a \times b \times c$, $a = b = c$)–T2($2a \times 2b \times c$, $c > a > b$), where a, b and c are unit cell parameters of the parent cubic cell, the M-point of the parent cubic phase has become a Γ-point, and below 913 K one can expect activation of the M-zone-boundary phonons in the Raman spectra. At the next transition to the T1($2a \times 2b \times 2c$, $c > a > b$) phase, additional folded phonons from the R- and X-points should

be also Raman active. However, apart from the above-mentioned disorder-induced bands, no new Raman lines were observed either in the T2 or in the T1 phase. According to [39], the magnitude of the plus tilts in the T2 and T1 phases is about 6°, while the minus tilt in the T1 phase is smaller (5°). Apparently, the structural changes that occurred in these phases induce relatively weak lattice distortions and do not provide high enough polarizability in Raman scattering processes for folded phonons. The absence of folded phonons in the Raman spectra in the T2 and T1 phases implies that the polarizability derivatives ($\partial\alpha/\partial q_{sm}$, where q_{sm} is the atomic displacement) of the corresponding soft modes are relatively small because octahedral plus and minus tilts involve only oxygen atoms. One can conclude that the high-temperature transitions display the displacive/order–disorder crossover, as already underlined by Gervais *et al* [27], and the combined effect of low-frequency phonons and correlated fluctuations could give rise to the particular x-ray patterns observed by Dénoyer *et al* [12]. Note that successive vanishing of the diffuse scattering at U–T2–T1–S phase transitions coincides with the abrupt transformation observed in our Raman spectra. As one can see in figure 4(a), relatively narrow Raman lines arise from the continuum (density of states) just below the S–R transition.

The following phase transitions to S, R and P_o phases are very likely associated with the condensation of the soft modes from the T ($\mathbf{q} = \frac{1}{2}\mathbf{b}_1 + \frac{1}{2}\mathbf{b}_2 + \mu\mathbf{b}_3$) line of the BZ. For these points the Lifshitz invariant is allowed for some irreducible representations. Thus, at lower temperatures, one may expect an INC phase to exist within the limited temperature interval. When the frequencies of the R_{25} and M_3 modes are simultaneously low, it is very probable that the frequency of the lowest-lying mode along the whole line T is also low. Ishida and Honjo [22] have shown that in NN the branch of the T_2 mode remains low and is entirely flat along the line T. A similar feature was also experimentally observed in $SrTiO_3$ [40, 41] and $RbCaF_3$ [42, 43]. The phonon dispersion relations of several cubic perovskites computed using first-principles variational density-functional perturbation theory also revealed a rather flat dispersion of the lowest-lying branch between the R- and M-points of the BZ [44]. Moreover, temperature-dependent minima on the optical branch at $\mu = 1/4$ and $1/3$ or even at arbitrary points inside the BZ may induce first-order phase transitions into the modulated (including INC) phases. In the modulated phases, the BZ folding activates many new Raman lines. Their number and frequency positions depend on the wavevector, which corresponds to the centre of the new BZ in each modulated phase. Accordingly, at T1–S–R–P_o transitions, we have observed several low-frequency lines, which exhibit abrupt changes at phase transitions.

Figure 4(a) illustrates the transformation of the low-frequency Raman spectra at T1–S–R–P_o transitions. As one can see in figure 4(a), the new Raman peak activated at the T1–S transition is rather broad and very likely consists of several unresolved components. The fitting procedure is hardly unique and at least three Raman peaks at about 30, 43 and 55 cm^{-1} should be included to fit the experimental line profile. Since all phases above room temperature are non-polar and contain a centre of symmetry, IR-active modes cannot be activated, and new lines can appear only due to the zone-folding effect. Apparently, folded T-modes activated in the S phase are very close in the frequency scale (very likely the dispersion of the lowest-lying soft branch is rather flat) and cannot be properly resolved. Moreover, taking into account possible contribution from BZ interior (Σ-, Δ- and Λ-points) one can expect rather complicated spectra. The observed activation of the folded modes suggests unit cell enlargement. Therefore, the unit cell of the S phase cannot be similar to that in the T1 phase ($2a \times 2b \times 2c$). The multiplicity $2a \times 4b \times 6c$ for the S phase (or $2a \times 6b \times 4c$) reported by Darlington and Knight [13] corroborates our observations. In the latter case the orthorhombic unit cell tripling along c and doubling along b at the T1–S transition would result in the activation of several Raman-active folded modes in the narrow frequency interval. Figure 4(b) shows a possible folding scheme at the T1–S transition.

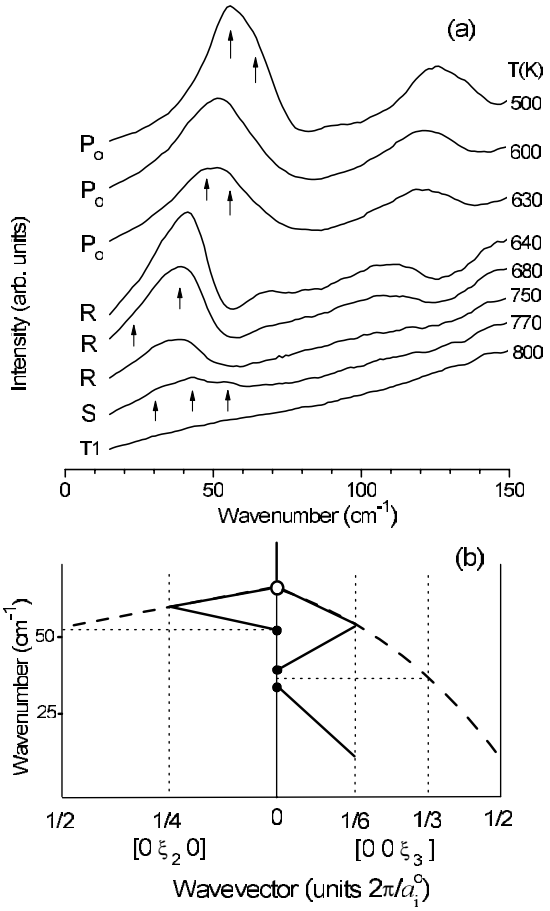

Figure 4. (a) Low-frequency Raman spectra (corrected for the temperature factor) in the temperature interval 500–800 K. Arrows indicate overlapped folded modes. (b) A possible folding scheme of the lowest-lying optical branches at the T1–S phase transition ($\xi_i = 2\pi/a_i^{\circ}$, $a_i^{\circ} \approx 2a_{\text{cubic}}$).

At the following transition to the R phase, the intensity of the low-frequency line abruptly increases, while its maximum shifts towards lower frequencies. As one can see in figure 4(a), the lowest-lying Raman peak activated in the R phase is asymmetric and contains at least two overlapped lines at about 20 and 40 cm^{-1}. One more line at 66 cm^{-1} is seen clearly. Obviously, these lines originate from the zone-boundary phonons associated with the octahedral tilts and octahedral distortions. Careful fitting performed by Bouziane *et al* [31] revealed three Raman lines at 20, 42 and 66 cm^{-1} in their (XX) spectrum recorded in the R phase (see figure 5 in [31]). Our fitting results presented in figure 5 are quite similar. In the R phase (temperature interval 636–753 K), the frequencies of these folded modes showed no remarkable temperature variation, while their intensity increases on cooling. Furthermore, two broad bands (230 and 620 cm^{-1} in the U phase) exhibit significant transformation on cooling down from 753 to 636 K. The former splits into several lines (at least six) while the latter exhibits downward shift. This band is asymmetric and consists of three overlapped lines at about 578, 610 and 650 cm^{-1}; the lowest one is the most intense. It is well known [10, 11] that the phase transition to the R phase is accompanied with the Nb displacement. Therefore, the observed transformation

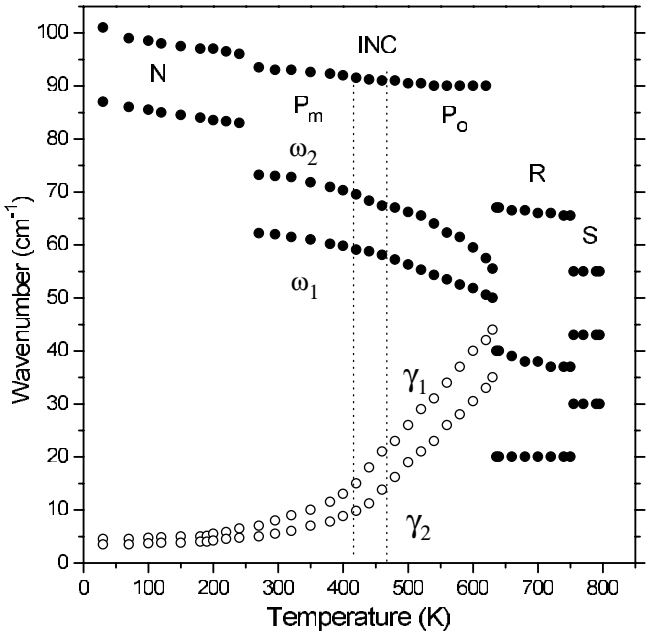

Figure 5. Frequencies (full symbols) and full width at half maxima (open symbols) of the lowest-lying folded modes in an NN single crystal.

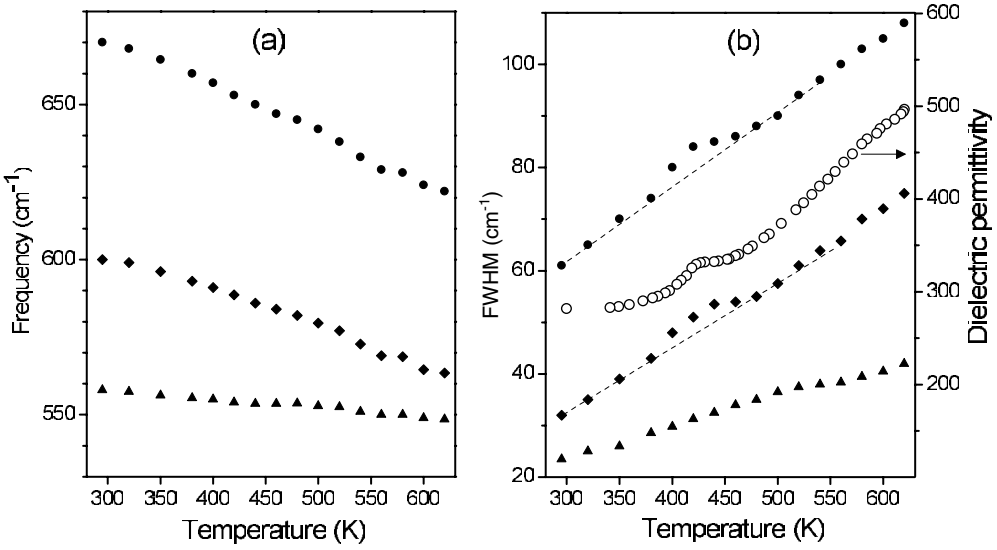

Figure 6. Temperature dependences of the frequency (a), full width at half maxima of Nb–O stretching modes (full symbols) and dielectric permittivity (open symbols) (b).

of the high-frequency Nb–O stretching band can be associated both with the folding of the corresponding optical branches and the changes in Nb–O bonding.

At the next transition to the P_o ($2a \times 4b \times 2c, c = a > b$) phase the tripling of the unit cell vanishes and the folding scheme changes abruptly. The lowest-lying folded Raman peak associated with the NbO_6 octahedral tilts appears at about 55 cm^{-1} and exhibits remarkable temperature dependence. Careful fitting in the temperature range 190–633 K showed that this lowest-lying peak is a doublet. The results are presented in figure 5. Two components (62 and

73 cm^{-1} at room temperature and 49 and 56 cm^{-1} at 630 K) are strongly overlapped above, approximately, 460 K. The latter fact was interpreted as evidence of a new phase transition in NN (see [12]). Recently, Bouziane *et al* [31] have shown that both components exist up to the P_o–R transition. Our results agree well with the temperature dependence reported in [31] and not with the results presented in [14]. It is worth noting that the line widths of the soft modes change the slope at, approximately, 400 K and increase considerably on further heating.

The temperature dependence of the high-frequency (500–700 cm^{-1}) bands is of particular interest. Bouziane *et al* [31] did not discuss this spectral range while Wang *et al* [14] observed three lines in this frequency range below 463 K and only two lines at higher temperatures. The observed vanishing of the 560 cm^{-1} line was interpreted as evidence of a new phase transition. We have performed detailed fitting in the temperature range 300–630 K and our results showed that all three lines exist up to 630 K. As shown in figure 6, their frequencies decrease (obviously, the Nb–O distance steadily increases) and all three lines exhibit broadening with increasing temperature. The second and third lines show abnormal behaviour in the temperature range 410–460 K. Their line widths increase linearly with increasing temperature while they deviate from the linear law between 410 and 460 K. The observed increased line width could be interpreted as a contribution from $q \neq 0$ because this temperature range coincides with the INC phase in NN [16]. As for any non-ferroelectric phase transition, the temperature dependence of the dielectric permittivity exhibits a change in the slope at about 460 K, which is the temperature of the normal–incommensurate transition. The following broad maximum at about 410–415 K corresponds to the 'lock-in' transition. The temperature dependence of the lattice parameters revealed the so-called invar effect in the same temperature range (figure 1). Dielectric, XRD and Raman measurements were performed on different samples and using different equipment; therefore, some shifts (a few degrees) in the temperature scale of course exist. Nevertheless, as one can see in figure 6, the dielectric anomaly and maximum of the temperature dependence of the line widths of the Nb–O stretching vibrations match very well.

The invar effect is a fingerprint of the INC modulation [45–48], and nearly constant (or even negative) thermal expansion in the *ac*-plane suggests the presence of INC modulation along the *b*-axis in NN. Since thermal expansion in crystals is caused by the anharmonic part of the interatomic potential the invar effect was explained as being due to competition between thermal vibrations and static atomic displacements in the modulated state. In the limited temperature interval the natural increase of the interatomic bond may be compensated via the tilt of this bond [48]. Our Raman data correlate well with the above scenario. As follows from figure 6, the frequencies of Nb–O stretching vibrations decrease, implying increasing of the corresponding bonds. The line widths of the stretching NbO_6 vibrations abnormally increase in the temperature interval 410–460 K, while the line widths of the tilting soft modes change slope at, approximately, 400 K and increase considerably on further heating. Together, the XRD and Raman measurements suggest that the INC modulation in NN can be described as rotations of the NbO_6 octahedra modulated along the *b*-direction.

As shown in figure 7, several strongly overlapped peaks in the intermediate frequency range (100–300 cm^{-1}) become better resolved on cooling. Their temperature dependence from room temperature up to the P_o–R transition was discussed in [14, 31, 32]. The fitting procedure is hardly unique because some peaks are very weak and overlapped with the neighbouring intense peaks. On heating above room temperature, all peaks in this range coalesce to give rise to a very complicated line shape [31], and it is not possible to estimate the temperature dependence of each peak properly. Note that the 120 cm^{-1} line is a singlet even at low temperature (190 K), and no splitting into 120–124 cm^{-1} components reported by Jimenez [32] was observed in our spectra. As one can see in figure 7, the Raman spectra above and below 460 K are markedly

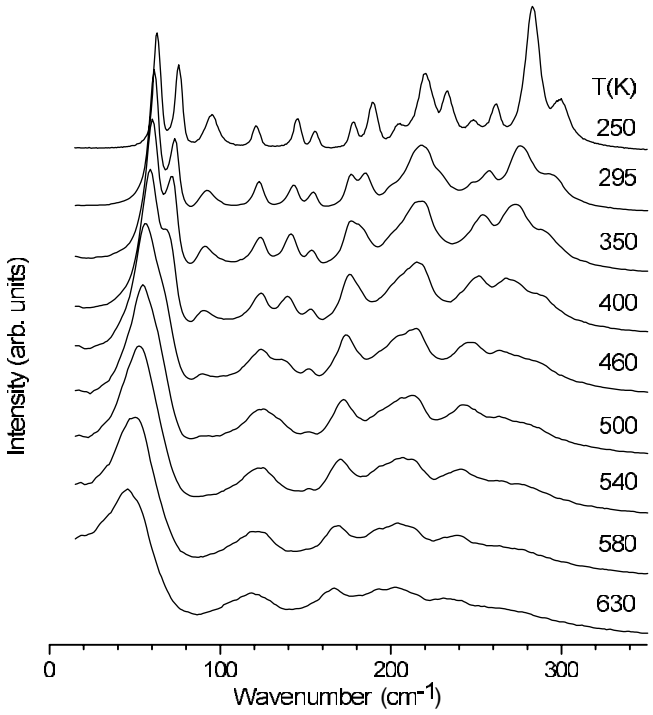

Figure 7. Low-frequency Raman spectra at various temperatures. Here the spectra are not corrected and can be compared with those reported in the literature [14, 29–32].

different and could imply symmetry lowering from orthorhombic (P_o) to monoclinic (P_m) via the INC phase on cooling, in agreement with the XRD data discussed above.

At the transition to the rhombohedral ferroelectric phase N the tilting scheme changes to $a^-a^-a^-$, while the unit cell multiplicity ($2a \times 2b \times 2c, a = b = c$) becomes similar to that in the T2 phase. According the tilt-system notations, recently introduced by Stokes *et al* [49], the distortions caused by ferroelectric displacements of the Nb cation along a given axis should be included as subscripts. Therefore, the correct tilting scheme for the C^6_{3v} group is $a^-_+a^-_+a^-_+$. Raman-active modes in the N phase originate either from the zone-centre phonons or from the R-point phonons of the cubic BZ. The corresponding factor-group analysis and correlation diagram via the intermediate D^6_{3d} group are presented in table 1. Note that IR-active zone-centre phonons become active in Raman scattering exclusively in the N phase. Therefore, of interest is a comparison of available IR spectra with the Raman spectrum in the N phase. In the cubic phase, the fundamental zone-centre modes were observed at 104 (TO_1), 411 (LO_1), 175 (LO_2; TO_2), 535 (TO_3) and 876 cm^{-1} (LO_3) at 1205 K [27]. On approaching the cubic–tetragonal U–T2 phase transition, the TO_1 soft-mode frequency squared departs from a linear law and starts to saturate, while the soft mode becomes overdamped ($\gamma_{sm}/\Omega_{sm} > \sqrt{2}$). The latter fact corroborates with the above-discussed disorder in the high-temperature phases.

Like in the Raman spectra, all bands in the room-temperature IR spectrum are essentially broad and overlapped [28]. Apparently, the possible splitting of the triply degenerated cubic modes is very small, while folded modes are very weak. The IR absorption spectrum consists of the broad high-frequency band at 620 cm^{-1}, three peaks in the intermediate frequency range at 360, 330 and 278 cm^{-1}, and strongly overlapped low-frequency bands. One band in the frequency interval 270–360 cm^{-1}, very likely, originates from the silent F_{2u} fundamental mode, which usually shows no splitting in the low-symmetry perovskites. The typical frequency

Table 1. Correlations of the vibrational representations from the Γ- and R-points of the parent cubic phase U to the Brillouin zone centre of the rhombohedral phase N.

The compatibility relations
$C_{3v}^6 \Leftarrow D_{3d}^6 \Leftarrow O_h^1 \Rightarrow D_{3d}^6 \Rightarrow C_{3v}^6$

$R3c$-C_{3v}^6	$R\bar{3}c$-D_{3d}^6	$Pm\bar{3}m$-O_h^1	$Pm\bar{3}m$-O_h^1	$Pm\bar{3}m$-O_h^1	$R\bar{3}c$-D_{3d}^6	$R3c$-C_{3v}^6
$\mathbf{k}=0$	$\mathbf{k}=0$	$\mathbf{k}=0$	$\mathbf{k}=\mu(\mathbf{b}_1+\mathbf{b}_2+\mathbf{b}_3)$	$\mathbf{k}=\frac{1}{2}(\mathbf{b}_1+\mathbf{b}_2+\mathbf{b}_3)$	$\mathbf{k}=0$	$\mathbf{k}=0$
A_1	A_{1g}	0 A_{1g}-[Γ_1]	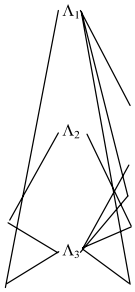	0 R_1-(A_{1g})	A_{1u}	A_2
A_2	A_{1u}	0 A_{1u}-[Γ'_1]		0 R'_1-(A_{1u})	A_{1g}	A_1
A_2	A_{2g}	0 A_{2g}-[Γ_2]		0 R_2-(A_{2g})	A_{2u}	A_1
A_1	A_{2u}	0 A_{2u}-[Γ'_2]		**1**R'_2-(A_{2u})	**1**A_{2g}	**1**A_2
E	E_g	0 E_g-[Γ_{12}]		0 R_{12}-(E_g)	E_u	E
E	E_u	0 E_u-[Γ'_{12}]		**1**R'_{12}-(E_u)	**1**E_g	**1**E
A_1+E	$A_{1g}+E_g$	0 F_{2g}-[Γ'_{25}]		**1** R'_{25}-(F_{2g})	**1**A_{1u} + **1**E_u	**1**A_2 + **1**E
1A_2 + **1**E	**1**A_{1u} + **1**E_u	**1** F_{2u}-[Γ_{25}]		**1** R_{25}-(F_{2u})	**1**A_{1g} + **1**E_g	**1**A_1 + **1**E
A_2+E	$A_{2g}+E_g$	0 F_{1g}-[Γ'_{15}]		0 R'_{15}-(F_{1g})	$A_{2u}+E_u$	A_1+E
4A_1 + **4**E	**4**A_{2u} + **4**E_u	**4** F_{1u}-[Γ_{15}]		**2** R_{15}-(F_{1u})	**2**A_{2g} + **2**E_g	**2**A_2 + **2**E

IR and Raman activity in the $R3c$-C_{3v}^6 phase:
4A_1 $(xx+yy; zz; T_z)$ + **5**A_2 (silent) + **9**E$(xx-yy, xy, xz, yz; T_x, T_y)$

value of the silent mode in perovskites ($SrTiO_3$, $KTaO_3$, $PbTiO_3$, $KNbO_3$ and $BaTiO_3$) varies between 266 and 308 cm^{-1}. In the rhombohedral phase N one can expect $4A_1 + 9E$ both IR and Raman active modes. According to the correlation scheme (table 1), at the direct U–N transition, the $3F_{1u}$ fundamental modes split into $A_1 + E$ doublets, while the silent F_{2u} mode splits into $A_2 + E$. Therefore, $3A_1 + 4E$ modes originate from the zone-centre modes, while $A_1 + 5E$ originate due to the zone folding. By comparing the Raman spectra in the P_m and N phases and taking into account the available IR data we have identified all peaks in the Raman spectrum at 30 K, as illustrated in figure 8. We attribute the low-frequency doublet (88, 101 cm^{-1} at 30 K), respectively, to E and A_1 components of the fundamental cubic TO_1 mode, which corresponds to Nb displacements with respect to oxygen octahedra. In $KNbO_3$, the TO_1 mode exhibits soft-mode behaviour and induces low-symmetry proper ferroelectric phases, while in NN this mode shows very weak temperature dependence and the frequency of the TO_1 mode in the N phase nearly coincides with that in the cubic phase. Thus, all phase transitions in NN are associated with the octahedral tilts, and Nb displacements are only secondary effects.

5. Conclusions

The competitive lattice instabilities at different points of the BZ induce a rather unusual sequence of phase transitions in NN. The octahedral tilts corresponding to the soft modes at the R- and M-points of the BZ are the primary order parameters, which induce the first two structural phase transitions from the cubic phase U into T2 and T1 phases in NN. The structural changes in the T2 and T1 phases induce relatively weak lattice distortions and do not provide high enough polarizability in Raman scattering processes for expected folded phonons. The Raman response of NN in the high-temperature U, T2 and T1 phases consists of two broad asymmetrical bands centred at about 230 and 620 cm^{-1}. The presence of these bands suggests significant disorder similar to that previously observed in $KNbO_3$ and $BaTiO_3$ crystals. On further cooling, NN exhibits a rather complicated phase transition sequence into modulated (including incommensurately modulated) phases because the lowest-lying branch

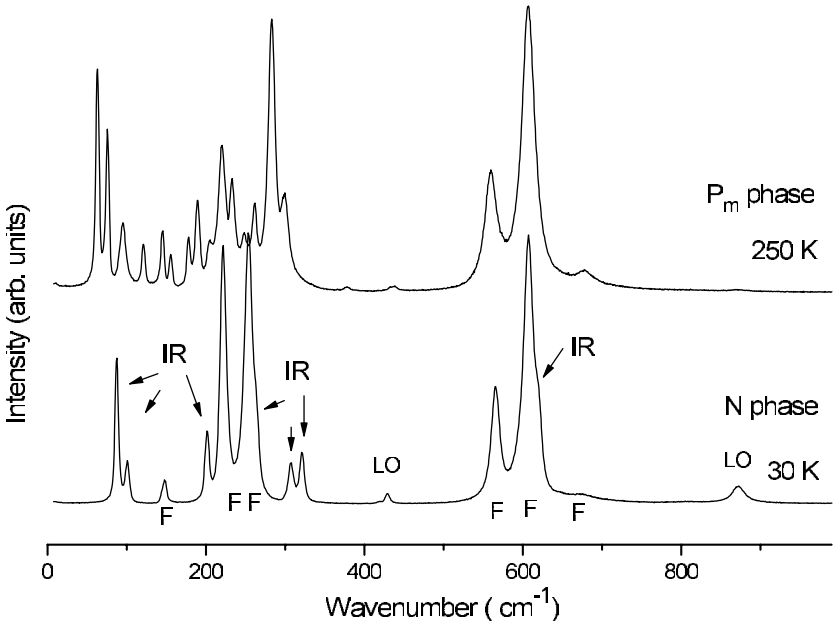

Figure 8. Raman spectra of NN at 250 K (P_m phase) and at 30 K (N phase). The arrows indicate phonons originating from the zone-centre IR active modes. Symbol F marks folded phonons.

along the whole line between the R- and M-points of the BZ softens. As a result of the BZ folding in the modulated S, R, P_o and P_m phases, the zone-boundary soft phonons associated with the octahedral tilts were observed in the Raman spectra. Although powder diffraction data enable us to make a precise determination of the unit cell multiplicities, the Raman data suggested significant unit cell enlargement in the S and R phases and corroborate the neutron diffraction investigations reported by Darlington and Knight [13]. XRD diffraction experiments revealed the invar effect in the temperature interval 410–460 K corresponding to the INC phase associated with rotations of the NbO_6 octahedra modulated along the *b*-direction. Our experiments suggest that the well-known phase P consists of three phases: monoclinic (P_m) between 250 and 410 K, INC between 410 and 460 K, and orthorhombic (P_o) between 460 and 633 K. The low-temperature transition to the ferroelectric rhombohedral N phase is caused by the condensation of the soft mode from the R-point accompanied by Nb displacements. All folded modes originating from the M- and T-points of the BZ abruptly disappear at the P_m–N transition. As a result, the Raman spectra in the N phase become much more simple and all peaks were assigned.

Acknowledgments

This work has been supported by the Russian Foundation for Basic Research (Projects 04-02-16228a, 05-02-16916a and 05-03-32214a).

References

[1] Lines M E and Glass A M 1977 *Principles and Applications of Ferroelectrics and Related Materials* (Oxford: Clarendon) chapter 8

[2] Tejuca L G and Fierro J L G (ed) 1993 *Properties and Applications of Perovskite-Type Oxides* (New York: Dekker)

[3] Mitchell R H 2002 *Perovskites: Modern and Ancient* (Ontario: Almaz Press)
[4] Cross L E and Nicholson B J 1955 *Phil. Mag.* **46** 453
[5] Sakowski-Cowley A C 1967 *PhD Thesis* University of Cambridge
[6] Sakowski-Cowley A C, Łukaszewicz K and Megaw H 1969 *Acta Crystallogr.* B **25** 851
[7] Glazer A M and Megaw H 1972 *Phil. Mag.* **25** 1119
[8] Ahtee M, Glazer A M and Megaw H 1972 *Phil. Mag.* **26** 995
[9] Darlington C N W and Megaw H 1973 *Acta Crystallogr.* B **29** 2171
[10] Glazer A M and Megaw H 1973 *Acta Crystallogr.* A **29** 489
[11] Megaw H D 1974 *Ferroelectrics* **7** 87
[12] Dénoyer F, Comès R, Lambert M and Guinier A 1974 *Acta Crystallogr.* A **30** 423
Dénoyer F, Comès R, Lambert M and Guinier A 1971 *Acta Crystallogr.* A **27** 414
[13] Darlington C N W and Knight K S 1999 *Physica* B **266** 368
[14] Wang X B, Shen Z X, Hu Z P, Qin L, Tang S H and Kouk M H 1996 *J. Mol. Struct.* **385** 1
[15] Raevskii I P, Reznichenko L A, Smotrakov V G, Eremkin V V, Malitskaya M A, Kuznetsova E M and Shilkina L A 2000 *Tech. Phys. Lett.* **26** 744
[16] Reznichenko L A, Shilkina L A, Gagarina E S, Raevskii I P, Dul'kin E A, Kuznetsova E M and Akhnazarova V V 2003 *Crystallogr. Rep.* **48** 448
[17] Ahtee M and Glazer A M 1974 *Ferroelectrics* **7** 93
[18] Shilkina L A, Reznitchenko L A, Kupriyanov M F and Fesenko E G 1977 *Sov. Phys.—Tech. Phys.* **22** 1262
[19] Henson R M, Zeyfang R R and Kiehl K V 1977 *J. Am. Ceram. Soc.* **60** 15
[20] Raevski I P and Prosandeev S A 2002 *J. Phys. Chem. Solids* **63** 1939
[21] Glazer A M 1972 *Acta Crystallogr.* B **28** 3384
[22] Ishida K and Honjo G J 1973 *J. Phys. Soc. Japan* **34** 1279
[23] Denoyer F, Comès R, Lambert M and Currat R 1976 *Solid State Commun.* **18** 441
[24] Darlington C N W 1975 *Phil. Mag.* **31** 1159
[25] Darlington C N W 1979 *Solid State Commun.* **29** 307
[26] Darlington C N W 2001 *Acta Crystallogr.* A **58** 66
[27] Gervais F, Servoin J L, Baumard J F and Denoyer F 1982 *Solid State Commun.* **41** 345
[28] Husson E and Repelin Y 1984 *Spectrochim. Acta* A **40** 315
[29] Shen Z X, Wang X B, Kuok M H and Tang S H 1998 *J. Raman Spectrosc.* **29** 379
[30] Lima R J C, Freire P T C, Sasaki J M, Ayala A P, Melo F F, Mendes Filho J, Serra K C, Lanfredi S, Lente M H and Eiras J A 2002 *J. Raman Spectrosc.* **33** 669
[31] Bouziane E, Fontana M D and Ayadi M 2003 *J. Phys.: Condens. Matter* **15** 1387
[32] Jiménez R, Sanjuan M L and Jiménez B 2004 *J. Phys.: Condens. Matter* **16** 7493
[33] Gailhanou M, Dubuisson J M, Ribbens M, Roussier L, Bétaille D, Créoff C, Lemonnier M, Denoyer J, Bouillot C, Jucha A, Lena A, Idir M, Bessière M, Thiaudière D, Hennet L, Landron C and Coutures J P 2001 *Nucl. Instrum. Methods Phys. Res.* A **467/468** 745
[34] Rodriguez-Carvajal J 1993 *Physica* B **192** 55 http://www-llb.cea.fr/fullweb/powder.htm
[35] Gagarina E S, Eknadiosyants E I, Reznichenko L A, Shilkina L A, Raevskii I P, Sakhnenko V P, Smotrakov V G and Eremkin V V 2002 *Crystallogr. Rep.* **47** 979
[36] Quittet A M, Bell M I, Krauzman M and Raccah P M 1976 *Phys. Rev.* B **14** 5068
[37] Fontana M P and Lambert M 1972 *Solid State Commun.* **10** 1
[38] Comes R, Lambert M and Guinier A 1968 *Solid State Commun.* **6** 715
[39] Darlington C N W and Knight K S 1999 *Acta Crystallogr.* B **55** 24
[40] Stirling W G 1972 *J. Phys. C: Solid State Phys.* **5** 2711
[41] Stirling W G and Currat R 1976 *J. Phys. C: Solid State Phys.* **9** L579
[42] Rousseau M, Nouet J, Almairac R and Hennion B 1976 *J. Phys. Lett.* **37** L33
[43] Rousseau M, Nouet J, Almairac R and Hennion B 1977 *J. Physique* **38** 1423
[44] Ghosez Ph, Cockayne E, Waghmare U V and Rabe K M 1999 *Phys. Rev.* B **60** 836
[45] Futama H J 1962 *J. Phys. Soc. Japan* **17** 436
[46] Khasanov S S and Shekhtman V Sh 1986 *Ferroelectrics* **67** 371
[47] Parsamyan T K and Shekhtman V Sh 1989 *Sov. Phys.—Solid State* **31** 69
[48] Bagautdinov B Sh and Shekhtman V Sh 1999 *Phys. Solid State* **41** 137
[49] Stokes H T, Kisi E H, Hatch D M and Howard C J 2002 *Acta Crystallogr.* B **58** 934